

NEW FORMULATION FOR CHAOTIC INTERMITTENCY WITH NOISE

Sergio Elaskar^{a,b,d}, Ezequiel del Río^c and Gustavo Krause^{a,b}

^a*Departamento de Aeronáutica, Universidad Nacional de Córdoba, Av. Velez Sarfield 1611, 5000 Córdoba, Argentina*

^b*CONICET*

^c*Departamento de Física Aplicada, ETSIA, Universidad Politécnica de Madrid, Plaza Cardenal Cisneros 3, Madrid, Spain*

^d*sergio.elaskar@gmail.com*

Keywords: Intermittency, Chaos.

Abstract. The proper description of turbulent flows presents difficulty for researchers in fluid mechanics. One feature of some of these flows is intermittency. The intermittency phenomenon in Chaotic Dynamics theory is understood as a specific route to the deterministic chaos when spontaneous transitions between laminar and chaotic dynamics occur. A correct characterization of the intermittency is very important, principally, to study those problems having partially unknown governing equations or there are experimental or numerical data series. In this paper a new methodology to investigate systems showing chaotic intermittency phenomenon with noise is presented. The methodology used for system without noise is extended to evaluate the noisy reinjection probability density (NRPD), the noisy probability of the laminar length and the noisy characteristic relation. The approach also provides information to accurately describe the noiseless system. It also was found that, for type-II and type-III intermitencies, for large values of the instability parameter the characteristic relations approach the associated ones to the noiseless intermittency. However, for low values of the instability parameter, the characteristic relations reach a saturation level that depends on the NRPD. Also, this new methodology does not need to satisfy noise strength lower than the control parameter, it allows to analyze the noise effect on the intermittency statistical properties for large noise strengths. However, in few cases for type-I intermittency, the description of the noiseless system using the noisy data can be inaccurate. In addition, it is shown that occasionally the presence of noise could be not detected due to the results behave as they would be corresponding to a noiseless system. This aspect may have important consequences especially when working with experimental data. To validate the new theoretical formulation, the analytical results are tested by several numerical computations, showing an excellent agreement between the analytical models and the numerical results.

1 INTRODUCTION

Intermittency is a particular route to chaos, where a transition between regular or laminar and chaotic phases occurs. In the intermittency phenomenon, when a control parameter exceeds a threshold value, the system behaviour changes abruptly to a larger attractor by means an explosive bifurcation (Nayfeh and Balachandran, 1995). Then, the periodic orbit becomes chaotic. The concept of intermittency was introduced by Manneville and Pomeau in (Manneville and Pomeau, 1979; Manneville, 1980), and it has been observed in several fluid dynamics topics such as plasma physics and derivative non-linear Schrodinger equation (Sanmartín et al., 2004; Sanchez-Arriaga et al., 2007); Lorenz system (Manneville and Pomeau, 1979; Manneville, 1980); Rayleigh-Bénard convection and turbulence (Manneville, 2004), etc. Also, intermittency has applications in other physical topics, such forced nonlinear oscillators; and in economical and medical sciences.

Classically, intermittency is classified into three different types called I, II and III (Schuster and Wolfram, 2005; Nayfeh and Balachandran, 1995) according to the Floquet multipliers or eigenvalue in the local Poincaré map. In intermittency type-I one of the Floquet multipliers leaves the unit circle through +1, there is a tangent bifurcation (Nayfeh and Balachandran, 1995). Intermittency type-II begins in a subcritical Hopf bifurcation or Naimark-Sacker bifurcation (Wiggins, 1990), therefore, two complex-conjugate Floquet multipliers or two complex-conjugate eigenvalues of the local Poincaré map exit the unit circle. Type-III intermittency is related to a subcritical period-doubling or flip bifurcation when one Floquet multiplier leaves the unit circle through -1.

By means of Poincaré sections it is possible to study the intermittency mechanism using maps. The local Poincaré maps for type-I, type-II and type-III intermittencies are respectively given by: $x_{n+1} = \varepsilon + x_n + a x_n^2$, $x_{n+1} = (1 + \varepsilon)x_n + a x_n^3$ and $x_{n+1} = -(1 + \varepsilon)x_n - a x_n^3$, where ε and a must be higher than 0. A fixed point of the local Poincaré map becomes unstable for positive values of a control parameter ε . Also, to generate intermittency it is necessary to have a reinjection mechanism that maps back from the chaotic zone into the local regular or laminar one. This mechanism is described by the reinjection probability density function (RPD), which is determined by the non linear dynamics of the system it self. Therefore, the accurate evaluation of the RPD function is extremely important to correctly analyze and describe the intermittency phenomenon. There was not an efficient method to obtain the RPD function. However, recently a more general RPD had been introduced (del Río and Elaskar, 2010; Elaskar et al., 2011; del Río et al., 2012; Elaskar and del Río, 2012; del Río et al., 2013, 2014; Krause et al., 2014a,b).

It is clear that noise affects all system dynamic, therefore it will be affect the RPD function. We note that in the previous studies about of the local noise effect is usually assumed that the noise strength σ is much smaller than ε . Here, we consider a general process where this hypothesis is not necessary and we define the noisy RPD function (NRPD).

2 FORMULATION FOR THE RPD FUNCTION

We consider a general one-dimensional map: $x_{n+1} = F(x_n)$. The RPD function, called here by $\phi(x)$, gives the statistical behavior of the reinjection trajectories, and it depends on the specific form of $F(x)$. The main concept to reach a more general formulation is given by the following integral (del Río et al., 2012):

$$M(x) = \begin{cases} \frac{\int_{\hat{x}}^x \tau \phi(\tau) d\tau}{\int_{\hat{x}}^x \phi(\tau) d\tau} & \text{if } \int_{\hat{x}}^x \phi(\tau) d\tau \neq 0 \\ 0 & \text{otherwise} \end{cases} \quad (1)$$

Where \hat{x} and c are the lower boundary of reinjection and the end of the laminar zone around of the unstable fixed point x_0 respectively. \hat{x} can be lower, equal or higher than zero. However, c is a constant verifying $c > 0$; and always the inequality $\hat{x} \leq x \leq c$ must be verify. Then, the laminar interval is defined by $[\hat{x}; x_0 + c]$. In the previous work (del Río and Elaskar, 2010) we used $\hat{x} = x_0$; however, a more general approach considering \hat{x} different to x_0 was established in (Elaskar et al., 2011). Note that the integral $M(x)$ smooths the experimental o numerical data series, and its numerical estimation is more robust than the direct evaluation of the RPD function, $\phi(x)$. Also, the practical evaluation of the function $M(x)$ is very simple, we can calculate it as:

$$M(x) \approx \frac{1}{n} \sum_{j=1}^n x_j, \quad x_{n-1} < x \leq x_n \tag{2}$$

where the reinjection points $\{x_j\}_{j=1}^N$ must be sorted from lowest to highest, i.e. $x_j \leq x_{j+1}$. We found that for a wide class of maps exhibiting intermittency, the function $M(x)$ satisfies a linear approximation:

$$M(x) = \begin{cases} m(x - \hat{x}) + \hat{x} & \text{if } x \geq \hat{x} \\ 0 & \text{otherwise} \end{cases} \tag{3}$$

where the slope $m \in (0, 1)$ is a free parameter. Then, using Eqs.(1 and 3) we can obtain the corresponding RPD:

$$\phi(x) = \lambda(x - \hat{x})^\alpha, \quad \text{with } \alpha = \frac{2m - 1}{1 - m} \tag{4}$$

where λ is a normalization constant and $\alpha > -1$ because $0 < m \leq 1$. Note that for $m = 1/2$ we recover the uniform RPD, $\phi(x) = cte$. Therefore, the new formulation is more general, and it includes the uniform reinjection as a particular case.

3 NOISE INFLUENCE

In this section we study the noise influence on the statistical properties of intermittency, and we follow the research published in (del Río et al., 2012). For instance, for type-II intermittency we use the following noisy map:

$$x'_{n+1} = \begin{cases} F(x_n) + \sigma\xi_n & x_n \leq x_r \\ (F(x_n) - 1)^\gamma + \sigma\xi_n & x_n > x_r, \end{cases} \tag{5}$$

ξ_n is a uniform distributed noise verifying that $\langle \xi_m, \xi_n \rangle = \delta(m - n)$ and $\langle \xi_n \rangle = 0$. Where σ is the noise intensity. To keep x'_{n+1} in the unit interval we modifies the the map as follows:

$$x_{n+1} = \begin{cases} |x'_{n+1}| & x'_{n+1} \leq 1 \\ |x'_{n+1}| - 2 \text{ mod}(|x'_{n+1}|, 1) & x'_{n+1} > 1. \end{cases} \tag{6}$$

We can note that when $\sigma = 0$, we recover the previously used map (Elaskar et al., 2014). Fig.(1) shows the reinjection mapping into the laminar region. The dashed arrow represents the noiseless trajectory. However, the trajectory for the system (5-6), due to the noise, may spread over a region enclosed by the solid lines. To analyze the noise influence in type-III intermittency, we use the following map:

$$x_{n+1} = -(1 + \varepsilon) x_n - a x_n^3 + d x_n^6 \sin(x_n) + \sigma\xi_n, \tag{7}$$

As fist step we calculate the function $M(x)$ for the map (5-6) considering two cases: with and

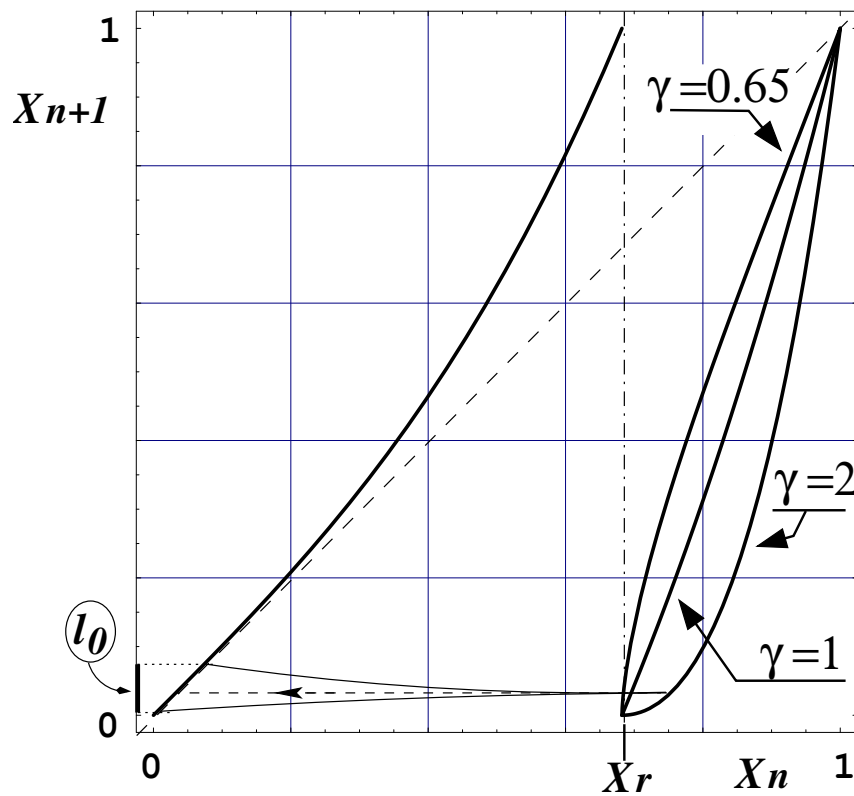


Figure 1: Map of Eqs.(5-6).

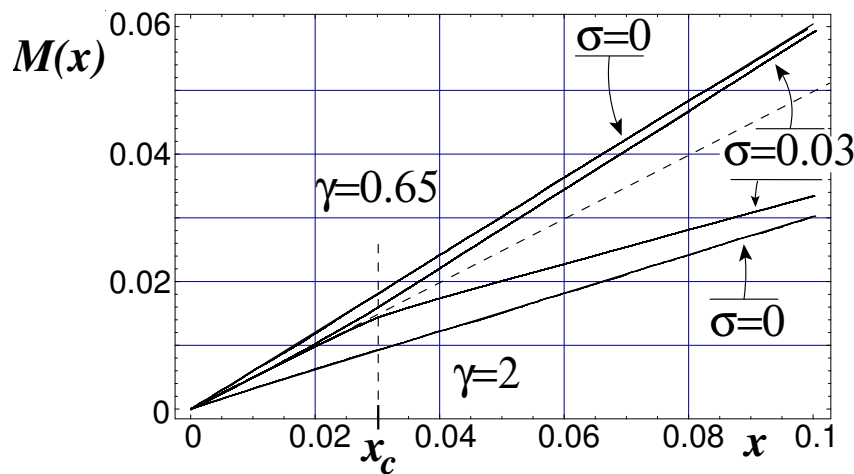


Figure 2: Numerical simulations of $M(x)$ for the map (5-6). The dashed line has slope $1/2$. The lines above the dashed one correspond to $\gamma = 0.65$. The same values of noise strength is used for the two lines below the dashed one, that correspond to $\gamma = 2$. For all the cases $\varepsilon = 0.001$ is fixed and $c = 0.1$.

without noise. The results are indicated in Fig.(2). The functions $M(x)$ for noise and noiseless tests are smooth because the definition of $M(x)$ smoothed the data. For the noisy tests $M(x)$ has different behavior on each side of x_c and it can be approximated by a piecewise linear function with two slopes. And the value x_c depends on the noise intensity, σ . For $x < x_c$ the slope of $M(x)$ approaches $1/2$, as we expect for the uniform reinjection. However, for $x_c < x$, the slope of $M(x)$ reaches a very similar value to the corresponding noiseless slope. For $\gamma = 0.65$ in the noisy test the slope is $m \approx 0.61$ and to the noiseless case $m \approx 0.60$. Then, in the region

$x_c < x$ the noisy RPD (NRPD) must have a similar form that the RPD function. This is a very important property of $M(x)$ because by means of the noisy data analysis we can obtain the RPD function for the noiseless case. We note that noise acts on the complete system. However, it does not affects the function $M(x)$ in the region $x > x_c$. Then, on the right side of x_c , the RPD function is robust against the noise but in the region $x < x_c$ the noise modifies the RPD. The noise influence, for $x < x_c$, produces that the RPD approaches to the uniform reinjection, at least locally around $x = 0$. For type-III intermittency, we find a similar behavior. The main difference happens in the value of x_c , that in this case it is bigger. We start with a numerical calculation of the function $M(x)$. The results are plotted in Fig.(3). We note that for values close to the origin (on the left of the arrows), the function $M(x)$ approaches $M(x) \approx 0.5x$, but for points on the right hand side of the arrows we have $M(x) \approx mx$ where the slope m is similar as to in the noiseless map. For the map with type-III intermittency the effect of noise on

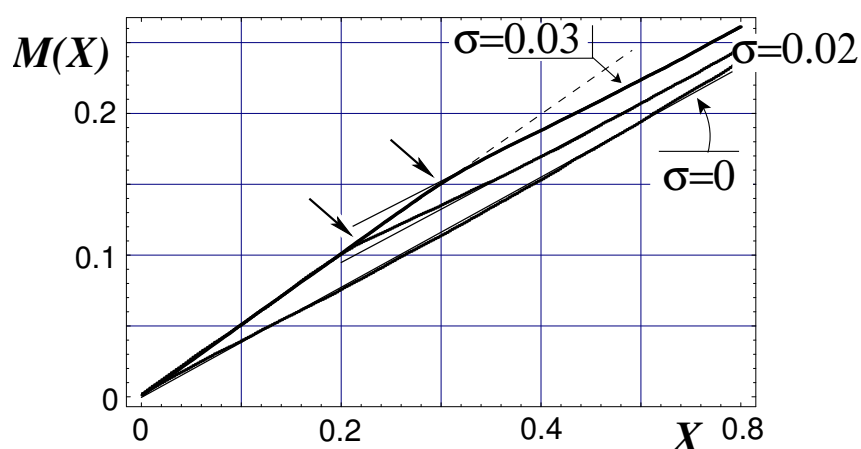


Figure 3: Function $M(x)$ for the map Eq.(7). The parameters are: $c = 0.8$, $a = 1.1$, $d = 1.35$, $\varepsilon = 10^{-4}$. Arrows show when $M(x)$ change the $1/2$ slope.

the function $M(x)$ is stronger than for the map with type-II intermittency because the transition from the 0.5 slope to a slope close to the noiseless test takes place for bigger values of x_c than for the type-II map.

3.1 Analytical NRPD in type II intermittency

To obtain an analytical expression for the NRPD, denoted by $\Phi(x)$, we analyse the effect of noise on the reinjection trajectories, as it is described in Fig.(1). A trajectory without noise is indicated by a dashed line, when this trajectory is perturbed by noise the reinjection point can be placed inside of the interval l_0 . That is, the noiseless density $\phi'(x)$ should be transformed into a new density $\Phi(x)$ according to the convolution:

$$\Phi(x) = \int \phi'(y)G(x - y, \sigma)dy \quad (8)$$

Where $G(x, \sigma)$ is the probability density of the noise term $\sigma\xi_n$ in Eq.(5). For $x > x_c$, the slope of the noisy $M(x)$ approaches the corresponding slope without noise, and we can calculate the function $\phi(x)$ without noise. These developments suggest that $\phi'(x) \approx \phi(x)$, where $\phi(x) = \lambda|x|^\alpha$ is the noiseless RPD. We note that the parameters λ and α are the values for the noiseless map. We introduce $\phi'(x) = \lambda|x|^\alpha$ in the convolution integral to prove this assumption. As

noise source we used a random variable ξ in the interval $[-1,1]$, hence its probability density G in Eq.(5) and (7) is given by

$$G(x, \sigma) = \frac{\Theta(x + \sigma) - \Theta(x - \sigma)}{2\sigma} \quad (9)$$

Where $\Theta(x)$ is the Heaviside step function. After solving the integral, we can write the NRPD function as:

$$\Phi(x) = \frac{1}{c^{1+\alpha}} \frac{(|x| + \sigma)^{1+\alpha} - Sg(|x| - \sigma)|x| - \sigma|^{1+\alpha}}{2\sigma}, \quad (10)$$

$Sg(x)$ is the sign function. In Fig.(4) we compare the results calculated by Eq.(10) with the numerical simulations for different noise levels. We consider the same values of m and α obtained from Fig.(2). We observe a good agreement between the numerical simulations and the analytical evaluations. However, when the intensity of the noise is higher we find differences of about 10 percent between the noiseless slopes m obtained with and without noise data. But, the power law exponential form of the RPD, $\phi'(x) = \lambda|x|^\alpha$, remains robust (del Río et al., 2012).

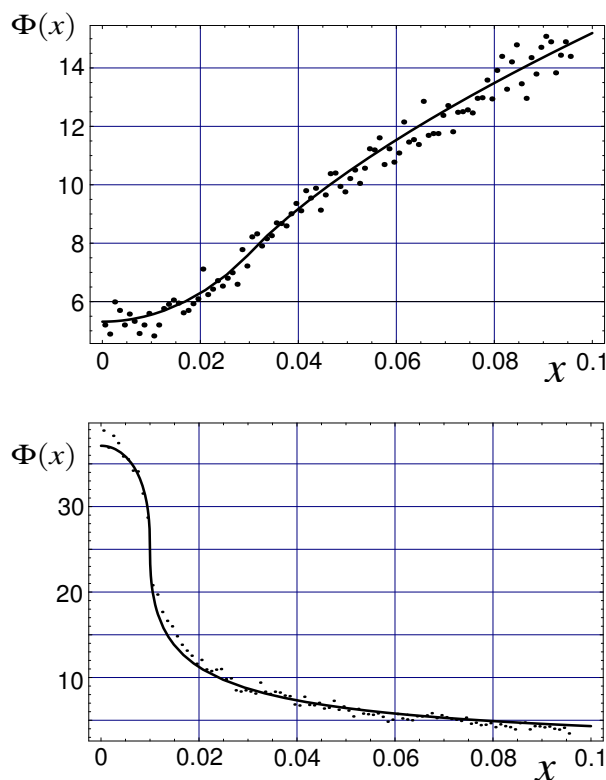


Figure 4: NRPD for the map Eq. (5-6). a) $c = 0.1$, $\gamma = 0.65$, $\sigma = 0.03$ and b) $c = 0.1$, $\gamma = 2$ and $\sigma = 0.01$. Dots correspond to numerical data, Eq.(10) is plotted as a solid line.

3.2 Analytical NRPD in type III intermittency

We show in the previous section that the noiseless RPD for type-III intermittency follows a power law. This law depends on the neighboring points of the map maximum and minimum values, Eq.(7), (Elaskar et al., 2011). In Fig.(5) we indicate using a dashed line the noiseless trajectory of a point starting near the maximum value of the map. When the noise affects the

system, this trajectory may spread over a region of some width, denoted here by l_0 . We can observe that l_0 will be stretched on the graph of the map by a suitable factor K , $l_1 = Kl_0$. The factor K depends of the particular form of the map. To reach an analytical equation for $\Phi(x)$, we consider that the map Eq.(7) can be represented by a composition of the two maps: one of them corresponds to a noiseless map $x'_n = -(1 + \varepsilon) x_n - a x_n^3 + d x_n^6 \sin(x_n)$, and the another is a new map $x_{n+1} = x'_n + \sigma \xi_n$. We use here a similar argument that for type-II intermittency,

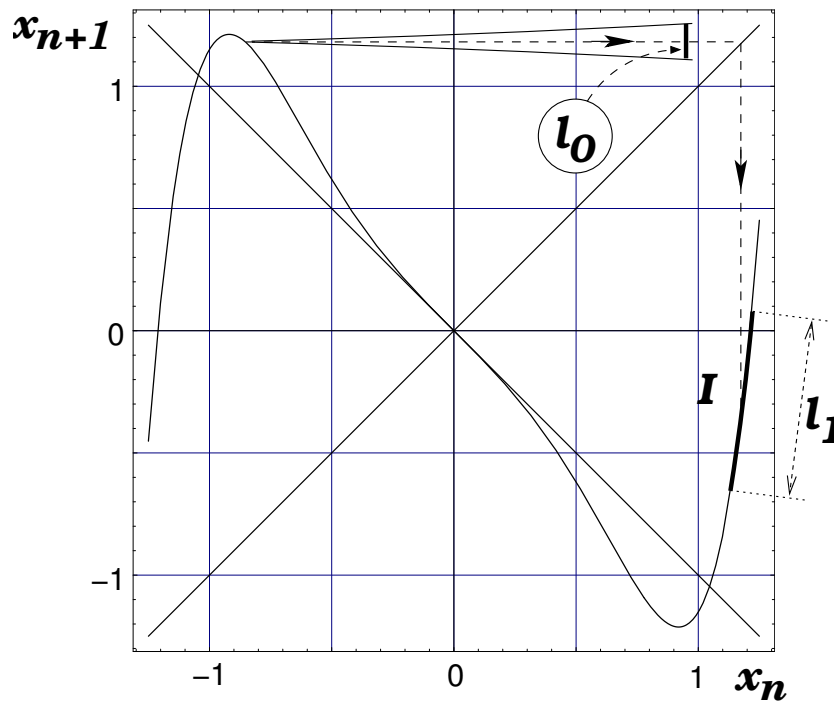


Figure 5: Map of Eq.(7). Dashed line indicates the effect of the map on a point near the maximum. Solid lines represent the noise effect on the same point.

and we consider that $\rho'(x)$ is the invariant density in a region close to the maximum of the map without noise. Then, the noise influence on this density can be obtained by means of the convolution $\rho(x) = \int \rho'(\tau)G(\tau - x, \sigma)d\tau$, where $\rho(x)$ is the invariant density in the interval l_0 . Unlike to the analyzed type-II intermittency test, for this type-III intermittency map, points placed on l_0 are not directly mapped on the laminar region. Therefore to obtain the NRPD, we must follow the evolution of the density $\rho(x)$ produced by the map (7) (del Río et al., 2012):

$$\Phi(x) = \frac{1}{c^{1+\alpha}} \frac{(|x| + K \sigma)^{1+\alpha} - Sg(|x| - K \sigma)||x|}{2K \sigma} - \frac{K \sigma^{1+\alpha}}{(2K \sigma)c^{1+\alpha}} \tag{11}$$

This expression is plotted in Fig.(6) showing agreement with the numerical results.

3.3 Analytical NRPD in type-I Intermittency

We use to represent the local map for type-I intermittency a quadratic map:

$$x_{n+1} = f(x) = ax_n^2 + x_n + \varepsilon, \tag{12}$$

where ε is the control parameter and it is the distance between the local Poincaré map and the bisectrix. The parameter a specifies the position of the point with zero-derivative. In the last

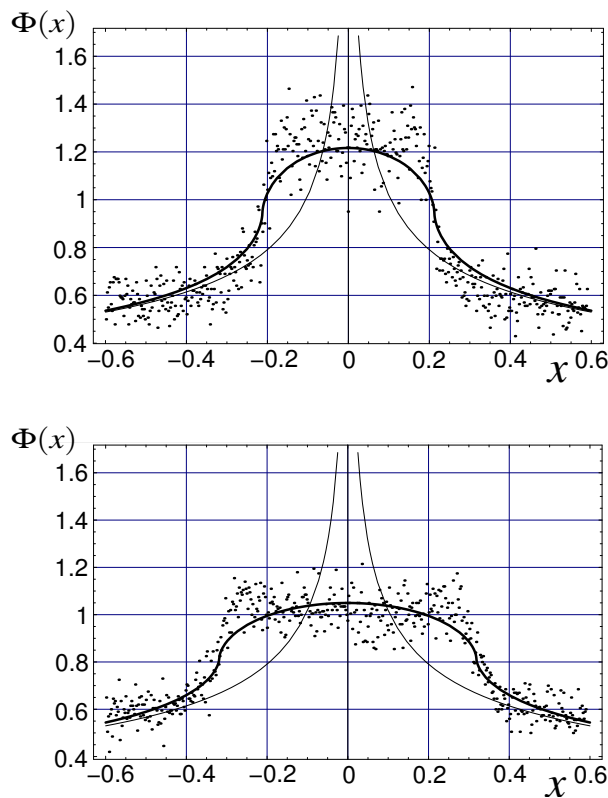


Figure 6: NRPD for two values of the noise strength σ of the Eq.(7): a) $\sigma = 0.02$ and b) $\sigma = 0.03$. Dots are numerical data whereas solid lines are given by Eq.(11). The noiseless RPD is also plotted. The parameters are: $c = 0.6, a = 1.1, d = 1.35, \varepsilon = 10^{-4}$.

equation, for $\varepsilon < 0$ there are two fixed point, one of them stable and other one unstable. For $\varepsilon = 0$ the two fixed points coalesce in one fixed point $xf = 0$; and for $\varepsilon > 0$ there are not fixed points. Furthermore, to have type-I intermittency must exist a reinjection mechanisms that return the trajectories from the chaotic zone into the local one. In this paper the non-linear map implmented by (del Río et al., 2013) is used:

$$g(x) = \hat{x} + h(x - x_m)^\gamma . \tag{13}$$

where \hat{x} is the lower boundary of reinjection (LBR). The LBR is here considered to be placed inside of the laminar interval $[-c, c]$. The coefficient h is obtained from $g(x_m) = \hat{x}$ and $g(f(x_m)) = f(x_m)$. Then, the global map can be written as:

$$F(x) = \begin{cases} f(x) = ax^2 + x + \varepsilon, & \text{if } x < x_m, \\ g(x) = \hat{x} + \frac{f(x_m) - \hat{x}}{(f(x_m) - x_m)^\gamma} (x - x_m)^\gamma + \sigma\xi_n & \text{if } x > x_m \end{cases} . \tag{14}$$

The exponent γ permits to obtain differents RPD functions. For $\gamma > 1$ the trajectories are concentrated around the \hat{x} point, therefore the RPD has a decreasing structure. However, for $0 < \gamma < 1$ the trajectories move away from the \hat{x} point, then the RPD function has an increasing form. For $\gamma = 1$, the RPD is approximatelly uniform.

The last term, $\sigma\xi_n$, represents the noise effect on the system. Where σ is the noise intensity, and ξ_n is a random variable which has an uniform probabily distribution.

In this paper is studied the noise effect on the global reinjection mechanism map excluding the local noise effect, which would reenter to the laminar region the orbits just leave it.

Figure 7 shows the map (14) for three different values of the exponent γ . Also, the noise effect and the *LBR* are indicated in this figure.

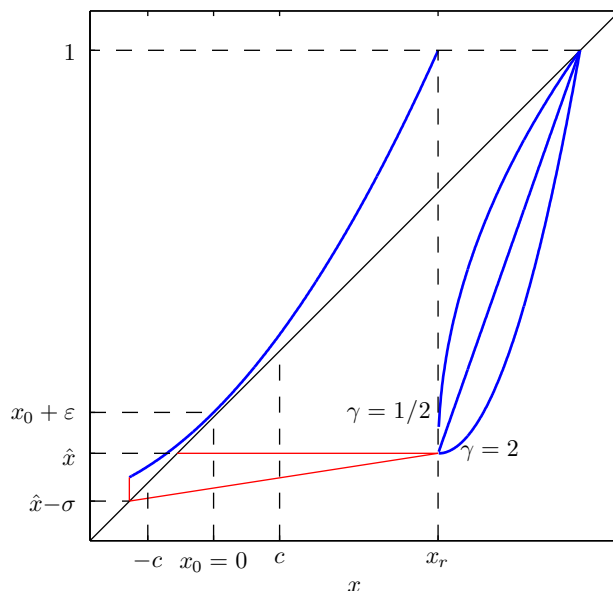


Figure 7: Eq. (14) for three values of γ . The new *LBR* produced by the noise effect is $\hat{x} - \sigma$.

The noise presence not only produces changes in the RPD due to the redistribution of reinjection points, but also it generates the displacement of the *LBR* point which is located in the new position $\hat{x} - \sigma$ (see Figure 7). This displacement results in a modification of the associated $\phi_l(l)$ function with respect to the noiseless results. In addition, if this displacement is such that $\hat{x} - \sigma < -c$, a discontinuity in the RPD function appears and consequently the $M(x)$ function will not be linear, therefore it is necessary to perform an adaptation of the previously presented methodology.

Although the noise is applied to the complete map, the associated power law to the RPD observed in the noiseless map, appears to be robust against noise, hence the noiseless $\phi(x)$ should be transformed into a new $\Phi(x)$ according to the convolution, see (del Río et al., 2012):

$$\Phi(x) = \int \phi(z) G(x - z, \sigma) dz, \tag{15}$$

where $G(x - z, \sigma)$ is the probability density of the noise term $\sigma \xi_n$ in Eq. (14).

We use a random variable ξ in the interval $[-1, 1]$ as noise source, hence the probability density G in Eq. (15) results:

$$G(x, \sigma) = \frac{\Theta(x + \sigma) - \Theta(x - \sigma)}{2\sigma}, \tag{16}$$

where Θ is the well known Heaviside function, which is equal to 1 for a greater than zero argument and otherwise cancels.

Initially assuming that $\hat{x} - \sigma > -c$ and considering Eqs. (15) and (16) we obtain

$$\Phi(x) = \frac{b}{2\sigma(\alpha + 1)} [(x - \hat{x} + \sigma)^{\alpha+1} - \Theta(x - \hat{x} - \sigma)(x - \hat{x} - \sigma)^{\alpha+1}] \tag{17}$$

The calculation of the exponent α can be made using the results of $M(x)$ function for noiseless reinjection points, i.e., the results of map (14) with $\sigma = 0$. Although the noiseless points are not available, the nonlinear noisy $M(x)$ function can still be used to calculate α . In Figure 8 noiseless and noisy results for $M(x)$ are shown.

We can observe that, as happened in types II and III intermitencies, in the region $x > \hat{x} + \sigma$ the noisy $M(x)$ is approximately linear with a slope similar to the noiseless case. This behaviour is independent of the parameter values, ε , \hat{x} and γ . Thus, it is possible to obtain the exponent α when the noiseless data is not available in the same way that in type II and III cases.

Note however, that in here, for $x < \hat{x} + \sigma$ the Heaviside function in Eq. 17 is zero and by changing the exponent α by $\alpha + 1$, we recover for $\Phi(x)$ the same power law than for $\phi(x)$. This is because the function $M(x)$ has two different slopes, that corresponds to exponents $\alpha + 1$ near \hat{x} and α far from \hat{x} . In this case, contrary to the type II and III cases, we can predict the behaviour of the noisy and noiseless system from the slope of the fuction $M(x)$ near the point \hat{x} .

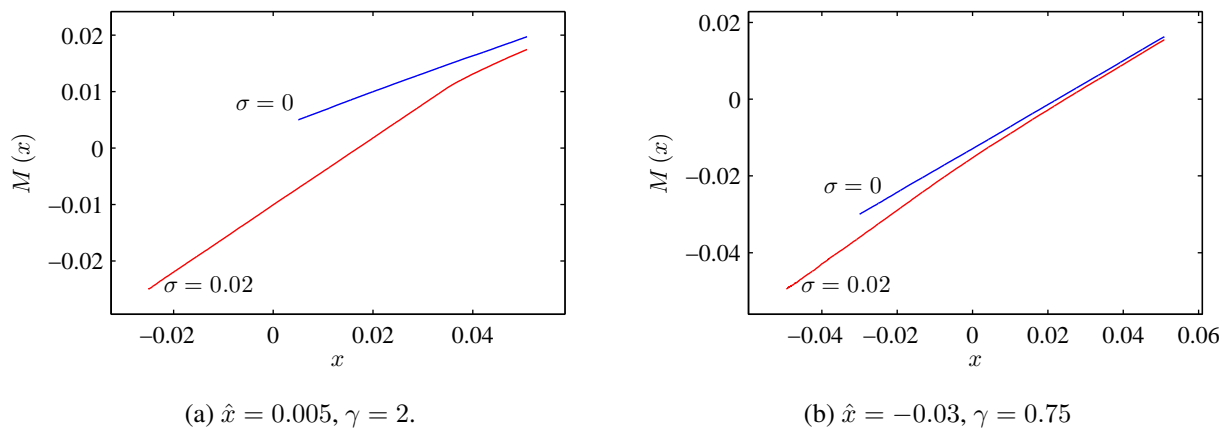


Figure 8: Comparison between the noisy and noiseless $M(x)$ function with $\varepsilon = 10^{-4}$, $c = 0.05$ and the indicated values. Note that for largest values of x the slopes are quite similar.

Eq. (17) models the noise effect on the reinjection points distribution for $\hat{x} - \sigma > -c$. When the displacement of the *LBR* goes beyond of the laminar interval left end, $\hat{x} - \sigma < -c$, a jump discontinuity appears in the NRPD, which is located in the point $F(-c)$. This occurs because the displacement $\hat{x} - \sigma$, below $-c$, generates that the trajectories going through points $x < -c$ always reinject in the region $x < F(-c)$, which produces a concentration of the reinjected points in the sub-interval $[x_z, F(x))$, where the point x_z is the lowest reinjection point, which depends on the noise level: for $F(\hat{x} - \sigma) < -c$, $x_z \equiv -c$, on the contrary for $F(\hat{x} - \sigma) > -c$, $x_z \equiv F(\hat{x} - \sigma)$.

Considering only points $x_z \leq x < F(-c)$, we always observed that the noisy $M(x)$ function is approximately linear in that region. Hence, we can assume a solution of the form:

$$\phi_2(x) = bk(x - x_z)^{\alpha_2}, \quad (18)$$

where b is the normalization parameter and the exponent α is calculated using the slope of points $x_z \leq x < F(-c)$. The coefficient k weighs the difference of proportion between the reinjection points coming from $x < -c$ and those coming from $g(x)$.

The function $\phi_2(x)$ is defined in the sub-interval $[x_z, F(-c))$. It is added to the solution (17) in that region in order to incorporate both effects on the NRPD, namely, the effect of re-distribution of the reinjection points due to noise and the effect of concentration in the left end of the laminar interval. For $\hat{x} - \sigma > -c$ there is no concentration, therefore $k = 0$ and then $\phi_2(x) = 0$.

Then, the NRPD function $\Phi(x)$ can be written as:

$$\Phi(x) = \begin{cases} \frac{b}{2\sigma(\alpha+1)} \left[(x - \hat{x} + \sigma)^{\alpha+1} - \Theta(x - \hat{x} - \sigma) (x - \hat{x} - \sigma)^{\alpha+1} \right] + & \text{if } x_z \leq x < F(-c), \\ b k (x - x_z)^{\alpha_2}, & \\ \frac{b}{2\sigma(\alpha+1)} \left[(x - \hat{x} + \sigma)^{\alpha+1} - \Theta(x - \hat{x} - \sigma) (x - \hat{x} - \sigma)^{\alpha+1} \right], & \text{otherwise,} \end{cases} \quad (19)$$

Where b is a normalization parameter. The calculation of the coefficient k is performed using the definition of function $M(x)$ as described below. For points $x > F(-c)$ the function $M(x)$ gives:

$$M(x) = \frac{\frac{1}{2\sigma(\alpha+1)(\alpha+2)(\alpha+3)} \left\{ (x - \hat{x} + \sigma)^{\alpha+2} [x(\alpha+2) + \hat{x} - \sigma] + (-\hat{x} + \sigma)^{\alpha+2} [x_{jmin}(\alpha+2) + \hat{x} - \sigma] + -\Theta(x - \hat{x} - \sigma) (x - \hat{x} - \sigma)^{\alpha+2} [x(\alpha+2) + \hat{x} + \sigma] \right\} + k(F(-c) - x_z)^{\alpha_2+1} \frac{F(-c)(\alpha_2+1) + x_z}{(\alpha_2+1)(\alpha_2+2)}}{\frac{1}{2\sigma(\alpha+1)(\alpha+2)} \left[(x - \hat{x} + \sigma)^{\alpha+2} - (x_{jmin} - \hat{x} + \sigma)^{\alpha+2} + -\Theta(x - \hat{x} - \sigma) (x - \hat{x} - \sigma)^{\alpha+2} \right] + k \frac{(F(-c) - x_z)^{\alpha_2+1}}{(\alpha_2+1)}} \quad (20)$$

being x_{jmin} the lowest reinjection point given by the greater of $\hat{x} - \sigma$ and $-c$.

The numerical values of $M(x)$ are known, therefore the k coefficient can be evaluated at any point $x > F(-c)$ in terms of the other parameters, which are also known:

$$k = \frac{(x - \hat{x} + \sigma)^{\alpha+2} \left[M(x) - \frac{x(\alpha+2) + \hat{x} - \sigma}{(\alpha+3)} \right] + (x_{jmin} - \hat{x} + \sigma)^{\alpha+2} \left[\frac{\hat{x}(\alpha+3) - \sigma}{(\alpha+3)} \right] + \Theta(x - \hat{x} - \sigma) (x - \hat{x} - \sigma)^{\alpha+2} \left[\frac{x(\alpha+2) + \hat{x} + \sigma}{(\alpha+3)} - M(x) \right]}{\frac{(F(-c) - x_z)^{\alpha_2+1}}{(\alpha_2+1)} \left[\frac{F(-c)(\alpha_2+1) + x_z}{(\alpha_2+2)} - M(x) \right] 2\sigma(\alpha+1)(\alpha+2)} \quad (21)$$

Finally the normalization parameter is obtained to complete all required values.

$$b = \left[\frac{k(F(-c) - x_z)^{\alpha_2+1}}{\alpha_2+1} + \frac{(c - \hat{x} + \sigma)^{\alpha+2} - (x_{jmin} - \hat{x} + \sigma)^{\alpha+2} - \Theta(c - \hat{x} - \sigma) (c - \hat{x} - \sigma)^{\alpha+2}}{2\sigma(\alpha+1)(\alpha+2)} \right]^{-1} \quad (22)$$

In Figures 9 and 10 we show results for different values of ε , \hat{x} , γ and σ , with $c = 0.05$. In these figures the numerical data (blue points) and the analytical approximation (red lines) are compared. We also show the corresponding noiseless results in order to clearly observe the effect of noise.

Figures 9 and 10 show a good agreement between the numerical data and the analytical approach for both, the NRPD and the probability density of the laminar lengths $\Phi_l(l)$. Note

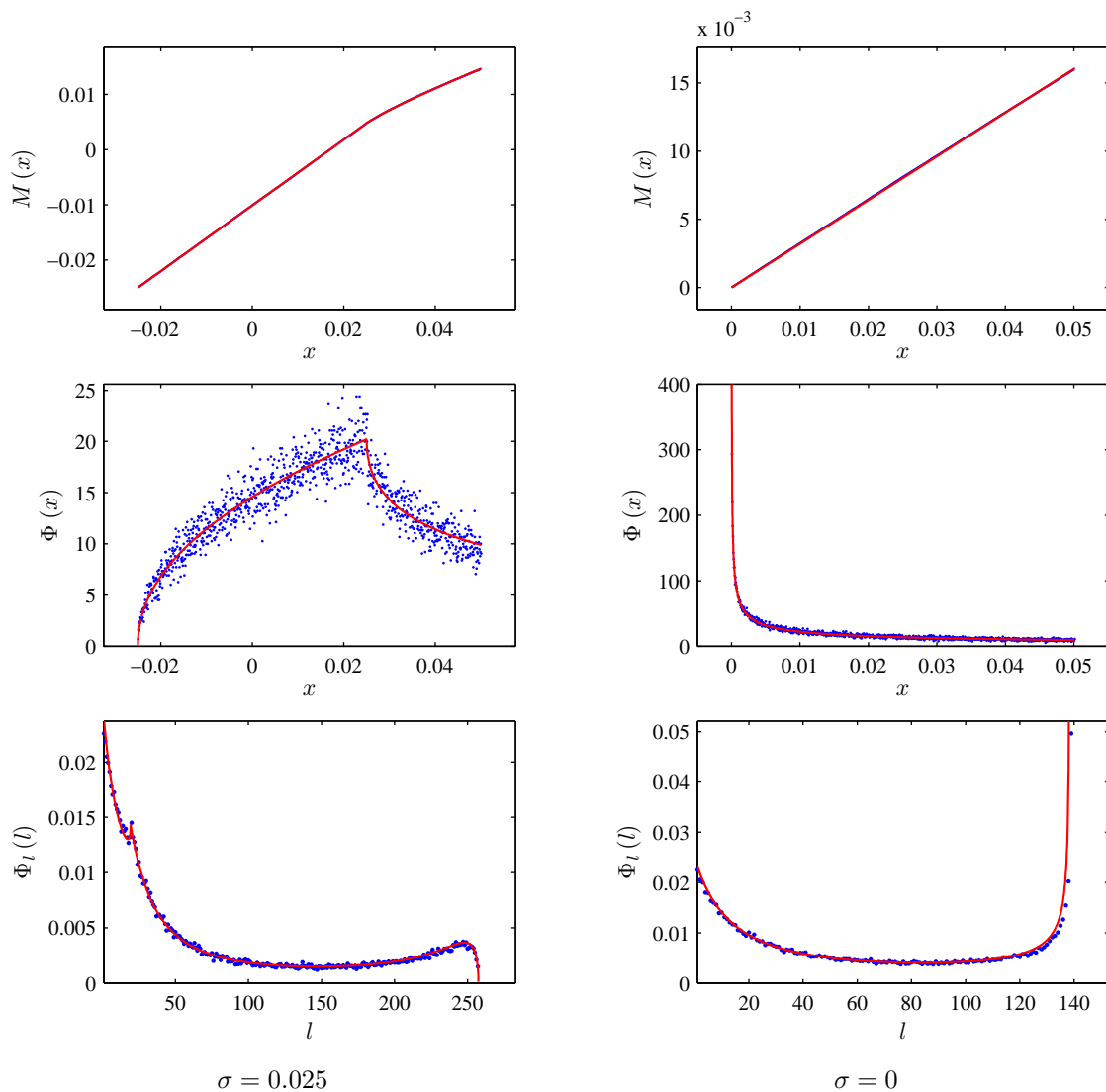


Figure 9: $M(x)$, NRPD and probability density of laminar lengths for map (14) with $\varepsilon = 10^{-4}$, $\hat{x} = 0$, $\gamma = 2$, $c = 0.05$ and the indicated noise levels. The slopes are $m = 0.320$ ($\alpha = -0.529$) for the noiseless case, $m = 0.596$ ($\alpha' = 0.479$) and $m = 0.331$ ($\alpha = -0.505$) for noisy $M(x)$ in each linear region.

the strong noise influence in the functions $M(x)$, $\Phi(x)$ and $\Phi_l(l)$. In the case of Figure 9, the feature $\phi(\hat{x}) \rightarrow \infty$ is replaced by $\phi(\hat{x} - \sigma) \rightarrow 0$ due to the noise presence, which also affects the density Φ_l that behaves as if would be $\alpha > 0$ with $\hat{x} < 0$ in the noiseless case (del Río et al., 2013).

In Figure 10 the functions $\Phi(x)$ and $\Phi_l(l)$ show the discontinuity described in the previously because $\hat{x} - \sigma < -c$. The jump in the probability density of the laminar lengths occurs at point corresponding to the maximum laminar length $l(-c, c)$ since all trajectories going through interval $[-c, F(-c)]$ need the same number of iterations to leave the laminar region.

Another important result deduced from Figures 9 and 10 is given by the relation between the slopes of both linear regions of $M(x)$. From Figure 9, we can observe that the exponent α' for the left region of the noisy $M(x)$, verifies the expression $\alpha' \approx \alpha + 1$, which is the same exponent of Eq. (19). This behaviour, which was verified by several simulations, implies that the slope of the noisy region of $M(x)$ does not depend on the noise strength, but is defined by the form of the return function (exponent γ).

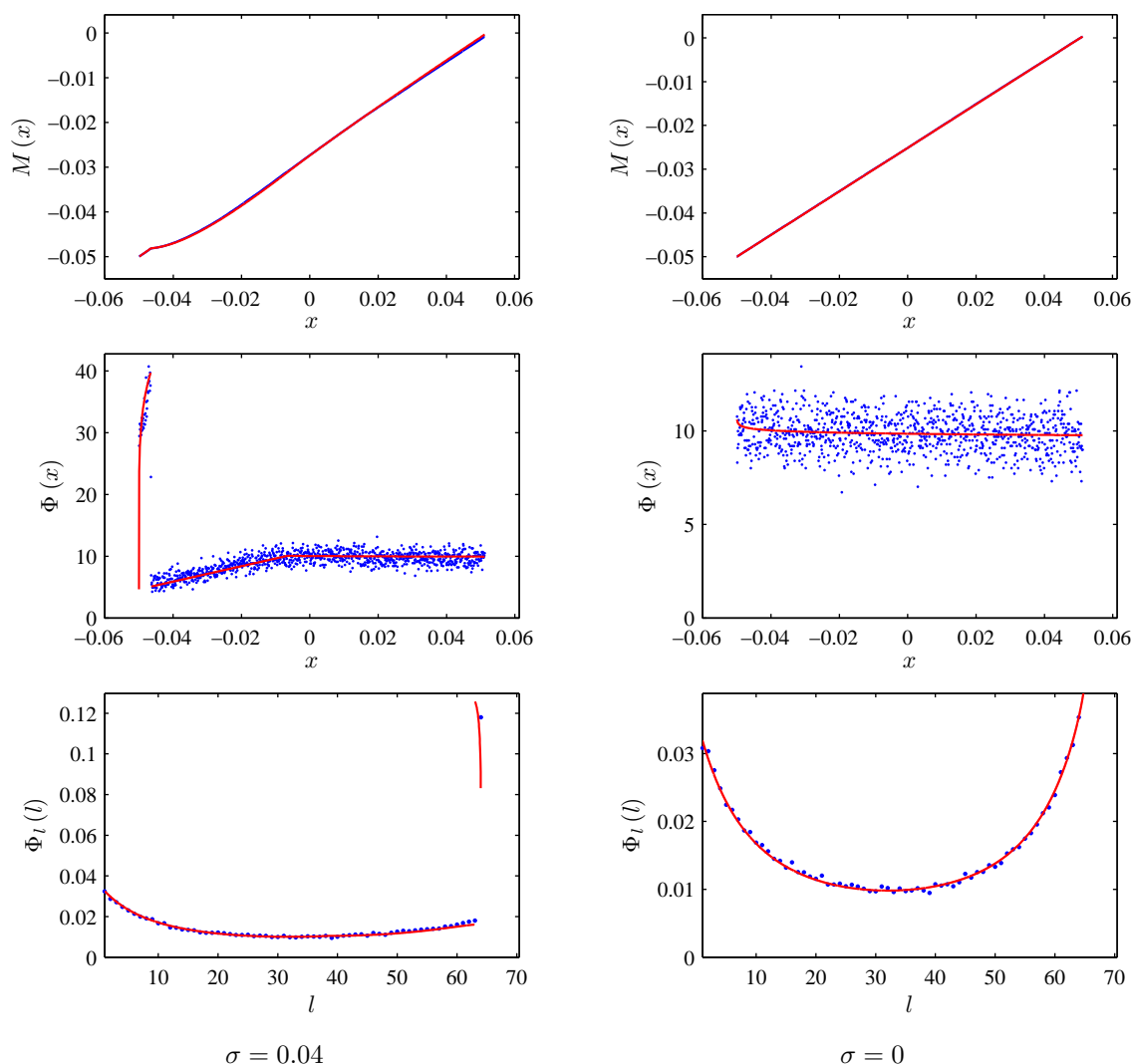


Figure 10: As Figure 9 with $\varepsilon = 10^{-3}$, $\hat{x} = -0.05$, $\gamma = 1$ and $c = 0.05$. In this case is $\alpha = -0.011$ (approximately uniform RPD for the noiseless case).

4 CONCLUSIONS

In this paper we have presented a review about of a new formulation for chaotic intermittency considering noise effects. This formulation is general and we have applied to type I, II and III intermittencies.

To evaluate the noisy reinjection probability distribution (NRPD) a function, called $M(x)$, is obtained previously. This function $M(x)$ is easier to calculate than the reinjection probability distribution; and the methodology implemented has been robust against noise.

Other studies have only considered that the control parameter is greater than the noise intensity ($\varepsilon > \sigma$). However, the methodology presented in this paper can be applied successfully when the noise intensity is greater than the control parameter ($\sigma > \varepsilon$).

Finally, we note that in all performed tests for type-I, II and III intermittencies, the numerical results and the theoretical formulation have shown a very good agreement.

REFERENCES

- del Río E. and Elaskar S. New characteristic relation in type-ii intermittency. *International Journal of Bifurcation and Chaos*, 20:1185–1191, 2010.
- del Río E., Elaskar S., and Donoso J. Laminar length and characteristic relation in type-i intermittency. 19:967–976, 2014.
- del Río E., Elaskar S., and Makarov V. Theory of intermittency applied to classical pathological cases. *Chaos*, 23:033112, 2013.
- del Río E., Sanjuan M., and Elaskar S. Effect of noise on the reinjection probability density in intermittency. *Communication in Nonlinear Sciences and Numerical Simulation*, 17:3587–3596, 2012.
- Elaskar S. and del Río E. Intermittency reinjection probability function with and without noise effects. *Latest Trends in Circuits, Automatics Control and Signal Processing*, 1:145–154, 2012.
- Elaskar S., S. del Río E., and Donoso J. Reinjection probability density in type-iii intermittency. *Physica A*, 390:2759–2768, 2011.
- Elaskar S., S. del Río E., and Krause G. New formulation for chaotic intermittency without noise. *Mecánica Computacional*, 44:En prensa, 2014.
- Krause G., Elaskar S., and del Río E. Noise effect on statistical properties of type-i intermittency. *Physica A*, 402:318–329, 2014a.
- Krause G., Elaskar S., and del Río E. Type-i intermittency with discontinuous reinjection probability density in a truncation model of the derivative nonlinear schrödinger equation. *Nonlinear Dynamics*, 2014b.
- Manneville P. Intermittency, self similarity and $1/f$ spectrum in dissipative dynamical systems. *Le Journal of Physics*, 41:1235–1243, 1980.
- Manneville P. *Instabilities, Chaos and Turbulence*. Imperial College Press, 2004.
- Manneville P. and Pomeau Y. Intermittency and lorenz model. *Physics Letter A*, 75:1–2, 1979.
- Nayfeh A. and Balachandran B. *Applied Nonlinear Dynamics*. John Wiley, 1995.
- Sanchez-Arriaga G., Sanmartín J., and Elaskar S. Damping models in the truncated dnls equation. *Physics of Plasmas*, 14:082108, 2007.
- Sanmartín J., López-Rebollal O., del Río E., and Elaskar S. Hard transition to chaotic dynamics in alfvén wave-fronts. *Physics of Plasmas*, 11:2026–2035, 2004.
- Schuster H. and Wolfram J. *Deterministic Chaos*. WILEY-VCH Verlag GmbH, 2005.
- Wiggins S. *Introduction to Applied Nonlinear Dynamical Systems and Chaos*. Springer-Verlag, 1990.